ELSEVIER

Journal of Nuclear Materials 241–243 (1997) 612–617

journal of nuclear materials

Core/divertor/wall particle dynamics in the DIII-D tokamak [1]

J.T. Hogan [a,*], R. Maingi [a], P.K. Mioduszewski [a], Th. Hutter [b], C.C. Klepper [a], M.R. Wade [a]

[a] *Oak Ridge National Laboratory, Fusion Energy Division, P.O. Box 2008, Oak Ridge, TN 37831-6376, USA*
[b] *Association EURATOM-CEA, DRFC, CE Cadarache, F-13108 St. Paul lez Durance Cedex, France*

Abstract

A wall model developed for the analysis of Tore Supra wall loading experiments has been applied to an experiment on DIII-D which demonstrated a substantial capacity for retention of deuterium gas in an all-graphite environment, and which showed the efficacy of the pumped divertor to deplete a gas-loaded wall. The Tore Supra model has been extended and applied to evaluate the particle exchange mechanisms between the core, divertor, and wall. Data-constrained plasma modeling is done for the discharges of the load/unload sequence. The poloidal distribution of the charge exchange flux profile to the divertor and outer wall is determined from the Eirene neutral transport code, to estimate the effective working areas for particle exchange and saturation. The deposition and saturation of the hydrogenic efflux in the aC:H layer and graphite is modeled with the 1-D WDIFFUSE code, applied to the regions fuelled by charge exchange flux to predict the instantaneous local wall recycling coefficient. A mechanism is proposed to explain the previous paradoxical result that exhaust quickly (~ 3 s) balances the only particle input, due to beam fueling, whereas a long term net wall depletion is observed over ~ 10 discharges. The saturation and depletion of wall layers fuelled by energetic charge exchange particles provides such a mechanism.

Keywords: Tokamak; DIII-D; Active pumping; Wall pumping

1. Introduction

The creation of fusion-relevant long pulse plasmas which can take advantage of recently discovered advanced confinement regimes requires that attention be paid to the mechanisms dominating particle control in steady state. On the technological side, present conditioning methods (e.g., helium glow discharge conditioning, HeGDC) are not feasible in superconducting devices and active wall exhaust is required. The cryopumping system on DIII-D permits investigation of the plasma/wall/pump interaction.

It has been observed on DIII-D that, when active pumping is started in saturated wall conditions, the exhaust flux quickly (~ 3 s) rises to a level which balances the only external fueling source, the injected neutral beams. Thus there is a prompt plasma-wall equilibration involving layers of only a few tens of angstroms at the surface [1].

DIII-D experiments have also been conducted in which an initially depleted wall, resulting from extensive HeGDC, was allowed to saturate in a sequence of neutral-beam and gas fuelled discharges without either active pumping or between-shots HeGDC. When the wall had saturated, active pumping discharges commenced, again without between-shots HeGDC. It was observed that the wall could be returned to a depleted state by active pumping over a number (~ 10) of discharges [2].

The results of this 'load/unload' experiment are, thus, paradoxical. While the wall apparently equilibrates rapidly (~ 3 s) so that the only fueling source (neutral beams) balances the exhaust by the pump, nevertheless net long term depletion of the wall is possible. The present work addresses the question of how and where a dynamic net

* Corresponding author. Tel.: +1-423 574 1349; fax: +1-423 576 7926; e-mail: hogan@fed.ornl.gov

[1] This research was sponsored in part by the Office of Fusion Energy, U.S. Department of Energy, under contract DE-ACOS-840 R214[00] with Martin Marietta Energy Systems, Inc.

PII S0022-3115(96)00574-0

wall depletion flux could originate in these 'load/unload' experiments.

A clue may be provided by previous analysis of experiments on long-pulse discharges in Tore Supra [3]. That analysis indicated the importance of charge exchange processes in core–wall particle exchange. The active pumping system in DIII-D operates in an all-graphite environment [4], so wall pumping is a competition between the passive graphite pumping and the active cryopumping system. Wall pumping has been previously analyzed with several semi-empirical models [5–7]. The latter work applied a model derived from analysis of the JET Preliminary Tritium Experiments (PTE). An upgraded version of the semi-empirical model is used to analyze the magnitude of wall pumping in the DIII-D experiments and evaluate the possible role of energetic charge exchange fluxes.

2. Description of DIII-D load / unload experiment

After reference discharges with between-shots HeGDC were established the HeGDC was ended and discharges without either HeGDC or cryopumping loaded the walls. A lower single null divertor configuration was used, with $I_p = 1.5$ MA, $B_t = 2.1$ T, $P_{NB} = 6.3$ MW, and ELMy H-mode conditions. The wall was judged to be saturated after 11 similar discharges when it became difficult to initiate the plasma discharge. Then the cryopump was activated and, after 10 similar pumping discharges, the D_α signal returned to a level previously attained with HeGDC, signifying a wall-depleted state. A particle inventory showed that the wall absorbed 8.8×10^{22} particles during the loading phase. Between-shots pumping of the gas was estimated to be small in comparison with the gas typically

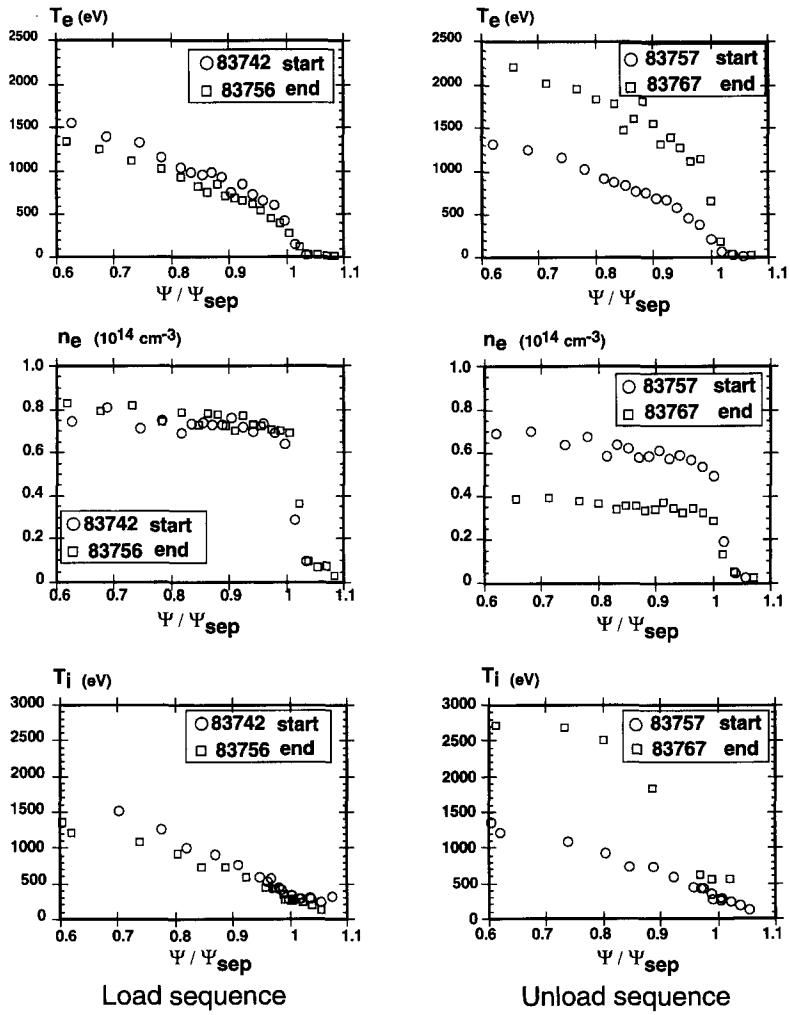

Fig. 1. Radial profiles of n_e and $T_{e,i}$ (from Thomson scattering and Charge Exchange Recombination). (a) (left) compares conditions at the beginning and end of the wall load phase, while (b) (right) compares profiles at the beginning and end of the unload (pumping) phase.

removed during pumping discharges. Further details of the load/unload experiment are given in Ref. [2].

3. Exchange process in DIII-D load/unload experiment

Since the graphite coverage area in DIII-D is 5.9×10^5 cm^2 [8] (taking account of openings for ports, etc.), an average areal deuterium atom density, assuming uniformity over the whole surface area, of 1.5×10^{17} at/cm^2 results from the 8.8×10^{22} particles absorbed. For fully saturated graphite ($n_D/n_C = 0.4$) this, in turn, would require a saturation depth (over the whole surface area) of ~ 300 Å. Assuming the average depth of deposition to be 0.6 Å/eV for D incident on C (consistent with the Moeller–Scherzer model [9,10]), the average irradiation energy required for a 300 Å depth is ~ 500 eV. This indicates that absorption by energetic particles must play a role, and that a depth greater than tens of Ångstroms is probably involved.

This supposition is reinforced by detailed examination of profile evolution during the sequence. Fig. 1 compares the radial profiles of n_e and $T_{e,i}$ for the sequence. Fig. 1a shows profiles for shot 83742 (beginning of wall loading) and 83756 (last shot before cryopumping). Loading produces a slightly higher central n_e and a slightly lower edge $T_{e,i}$. As discussed in Ref. [2], most of the change in recycling conditions occurred in the first shot of the sequence, indicating a rapid saturation of surfaces exposed to high particle fluxes. Fig. 1b shows the comparison between the first and last pumping discharges. The density is reduced substantially with a resulting higher $T_{e,i}$.

4. Wall/plasma model

The possible release mechanisms in graphite have been classified [11] as thermal detrapping from traps, diffusion through the surface and into the bulk (either from erosion dominated surfaces or from codeposition regions), recombination at the plasma-facing component and at the rear surface, and diffusion into the bulk and recombination at surface. The suitability of these mechanisms has been discussed in connection with similar experiments in JET Ref. [12].

The wall model used here, incorporating these processes, consists of a semiempirical one-dimensional diffusion equation solving for the hydrogenic diffusion in the aC:H layer in the divertor region. The model is similar to that used in Refs. [3,5] but revised to account for the results of Ref. [7]. As was shown in Ref. [2], the between-shots outgassing for this sequence followed a $t^{-0.7}$ dependence, similar to that observed in the Tore Supra load experiments, and in JET Ref. [12]. Since estimates for the

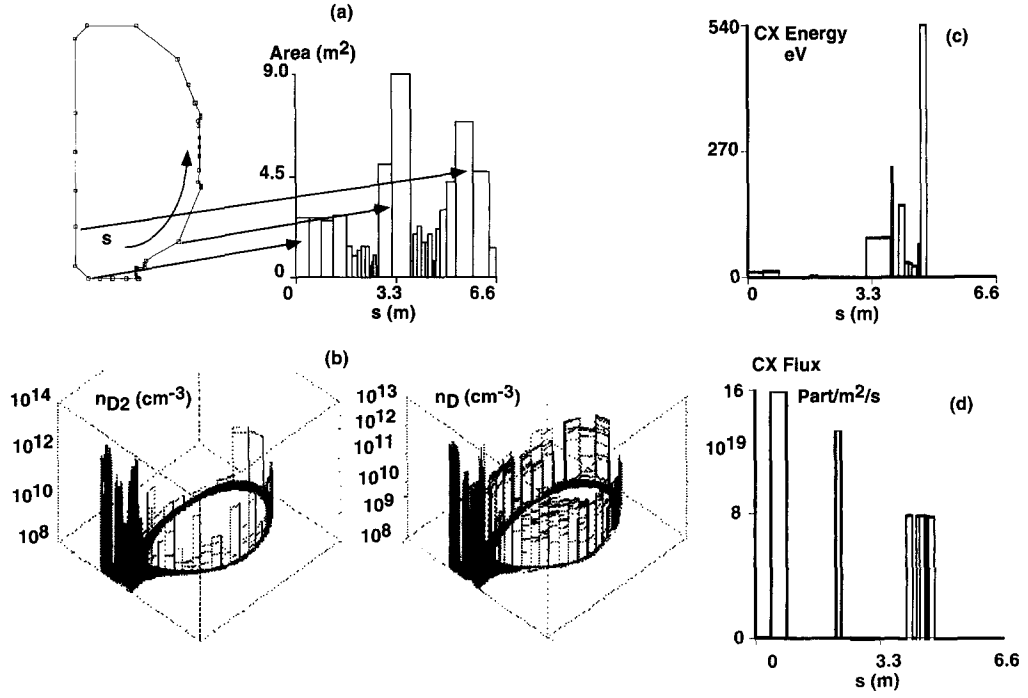

Fig. 2. Representative distributions of charge exchange fluxes defining the charge-exchange 'footprint' away from the divertor plates. The geometry and distribution of areas receiving fluxes (a), spatial distribution of D and D_2 density (b), the magnitude of the charge exchange flux (c), and the average energy of this flux (d) are shown.

diffusivity of hydrogen in graphite can vary by several orders of magnitude at a given wall temperature [13], it seems reasonable to assume the PTE values for wall properties with the additional step of calculating the localized deposition of fast particles during the sequence using measured profiles.

We treat deposition, diffusion, and emission from the surface with coupled equations for the concentrations of trapped (mobile) particles $C_{t,s}$

$$\frac{dC_s}{dt} = D\frac{d^2C_s}{dx^2} + \Phi\delta(x - x_0) - \Gamma C_s^2 - \frac{dC_t}{dt}$$

$$\frac{dC_t}{dt} = \frac{1}{\tau_a}C_s(1 - C_s/C_{0t}) - \frac{1}{\tau_a}\beta C_t - \sigma\Phi U(x - x_0)C_t$$

where the diffusivity, $D = 5 \times 10^{-19}$ m^2/s, and a surface recombination coefficient $K_r = 5 \times 10^{-37}$ m^4 s^{-1} from Ref. [7]. The spatial deposition source Φ describes incident ion implantation.

The saturation state of the plasma-facing surfaces has been estimated by using data constrained analysis of the neutral transport and deposition. The n_e and $T_{e,i}$ measurements (Fig. 1) provide the radial plasma profiles, while divertor plate thermal and Langmuir probe measurements help determine the local recycling parameters. The divertor plate saturates very quickly, within 100–200 ms because of the high local fluxes [14]. The saturation rate of other areas has been estimated using neutral transport calculations. Fig. 2 shows typical neutral distributions for DIII-D using the Eirene neutral transport code [15] with parameters from Langmuir probe (n_e, T_e) and IRTV (profile) measurements. Fig. 2 also shows the distribution of fluxes received in the charge-exchange 'footprint' areas around the poloidal circumference. While peak fluxes of 1.5×10^{20} m^{-2} s^{-1} are received from low energy particles near the strike points, fluxes of 7×10^{19} m^{-2} s^{-1} can be expected in the areas receiving significant fluxes of higher energy charge exchange particles. Thus the long term (more than one discharge) depletion or saturation characteristics can be determined by the degree of saturation of surfaces which are irradiated by energetic particles, away from the strike points. The direct neutral beam charge exchange halo neutral flux is not included in the Eirene example, but this gives a source of ~ 10 Torr l s^{-1} (or 1.4 Pa m^3 s^{-1}) localized around the midplane.

In order to estimate the wall deposition distribution, the energy spectrum of charge exchange particles is required. The one-dimensional SPUDNUT code has been used [16] to calculate the energy spectrum, based on measured radial plasma profiles. The calculations are carried out using the plasma radial profile information at selected intervals in the load/unload sequence. Profiles for shots 83742 and 83744 are used to characterize the depleted stage. Profiles from shot 83756 characterize the end of the load phase and profiles for 83745–83755 are interpolated linearly between those of 83744 and 83456. Similarly, shot 83757 is used to characterize the beginning of the unload phase, and 83767 the end of this phase. The rapid evolution during the first shots of the pumping sequence taken into account by assuming a nonlinear interpolation.

5. Results of calculation

Fig. 3 shows the calculated evolution of wall deposition during the discharge sequence. The deposition is calculated for each discharge in the sequence, using the assumptions described, and the shallow ($\Delta < 40$ Å), intermediate (40 Å $< \Delta <$ 150 Å) and deep ($\Delta > 150$ Å) deposition behavior is plotted. The shallow deposition behavior reflects the situation in the quickly saturated layers ($R \sim 1$). When pumping starts (and with it the density drop and T_i rise)

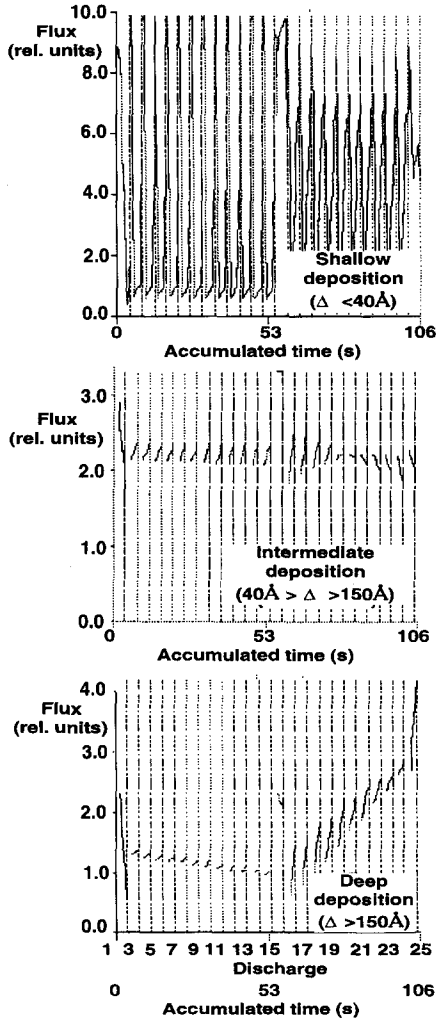

Fig. 3. Calculated evolution of shallow ($\Delta < 40$ Å), intermediate (40 Å $< \Delta <$ 150 Å) and deep ($\Delta > 150$ Å) CX deposition for the shots in the DIII-D load–unload sequence.

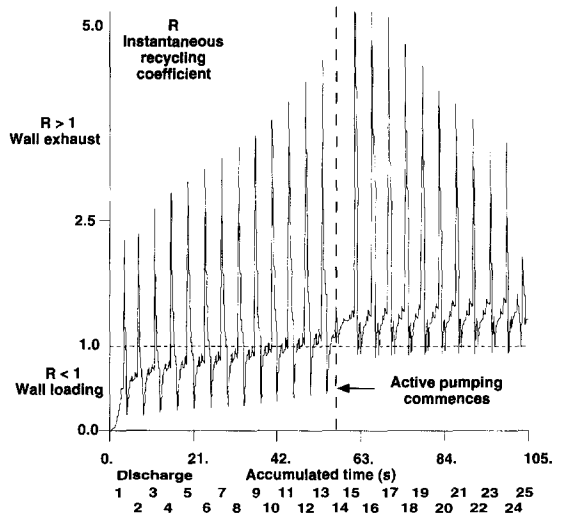

Fig. 4. Time variation of the calculated instantaneous recycling coefficient for the charge exchange active layer (from the WDIF-FUSE wall model) as this layer makes the transition from a depleted to a saturated state, then returns toward the depleted state after active pumping commences.

there is an increase in the deeper layer deposition from energetic particles. Note that the magnitude of the shallow deposition is much larger than that of the deeper fluxes and so small changes in the larger flux can mask large changes in the deep flux. The calculated spatial deposition profiles are used as input to the ID wall diffusion model.

Fig. 4 shows the evolution of the calculated instantaneous recycling coefficient (Φ_{out}/Φ_{in}), using the deposition fluxes just described, for the whole shot sequence. During the loading phase, the near surface region saturates (reaching $R \sim 1$). Note, though, that there is net trapping of the charge exchange flux (instantaneous $R < 1$) even while most plasma-facing components are already saturated and the overall recycling coefficient $R \sim 1$. When the deep region becomes increasingly saturated during the early stages of pumping, however, the instantaneous value of $R > 1$ and the previously deposited charge exchange flux can now be recycled to be exhausted by the cryopumping system.

6. Comparison with Tore Supra wall loading experiments

In the Tore Supra experiments described earlier, extensive (~ 70 h) HeGDC was performed to deplete the wall after machine operation in hydrogen. This was followed by a series of identical deuterium discharges which were run on the inner wall, after startup on an outboard limiter, as described in Ref. [3]. Fig. 5 (a detail not described in Ref. [3]) shows the measured time evolution in the hydrogen and deuterium energetic ($E_0 > 1$ keV) charge exchange fluxes for discharges during the sequence, as the wall evolved from an initial depleted state (shot 5068) to the near-density-disruption state (shot 5085). As can be seen, the deuterium charge exchange flux rises promptly in all cases when the plasma moves to the inner wall, indicating the dominant effect of the near surface saturated layer on the majority deuterium recycling, while the hydrogen charge flux shows an ever-slowing rise time, indicating its origin from an increasingly deeper saturated layer.

Using the wall diffusivity inferred from the outgassing analysis of these Tore Supra discharges [7] ($D = 5 \times 10^{-19}$ m^2/s) and assuming the hydrogen flux comes from a uniformly saturated layer of depth Δ ($\equiv (0.1 D\tau_{rise})^{1/2}$) the depth increases from 10 to ~ 50 Å during this sequence of ohmic shots. Assuming that the penetration depth is ~ 0.6 Å/eV, this would mean that the hydrogen recycling flux originates from regions saturated previously by fluxes of ~ 15–80 eV, characteristic of ohmic discharges, consistent with the analysis of the DIII-D load/unload experiments.

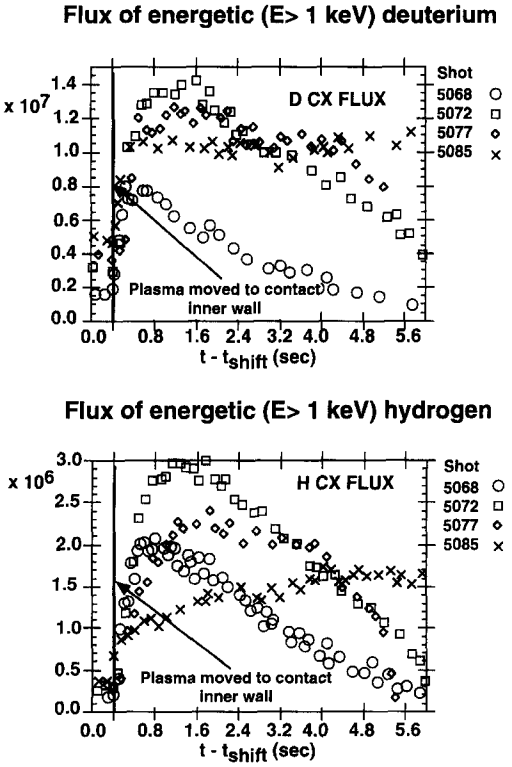

Fig. 5. Measured time dependence of hydrogen and deuterium energetic charge exchange fluxes ($E > 1$ keV) in Tore Supra inner wall loading experiments. The deuterium fluxes have a similar, prompt, rise time for all shots, while for the hydrogen the prompt rise seen early in the sequence gives way to an increasingly slower response, indicating a source deeper in the wall.

7. Discussion

A mechanism is thus found for particle exhaust by the cryopumping system. It provides a possible explanation for the salient, but hitherto unexplained feature of the DIII-D load/unload experiment. The paradox, that the particle exhaust quickly equilibrates to balance the neutral beam input, but that there is nonetheless a long term net depletion of the wall, would occur, in this model, because the long term wall depletion is dominated by the dynamics of layers which are populated by the energetic charge exchange flux. During the pumping, or unload, phase of the sequence these layers are irradiated because of the lower n_e, and corresponding higher T_i near the edge, which hardens the charge exchange efflux. This mechanism provides the required additional flux from the wall, in addition to the rapid equilibration of the near surface layers. While the quick equilibration of the exhaust and beam input involves only the 10–30 Å layers, deeper (> 300 Å) layers must be involved if only because of the gross magnitude of the particle deposition during the loading phase, which requires a depth of 300 Å, averaged over the entire plasma-facing surface.

It is evident that this proposed mechanism is far from established, and requires much more detailed and specific experimental investigation to confirm it. In particular, analysis with species-specific hydrogenic charge-exchange diagnostics, like those utilized in the Tore Supra wall loading series (results are shown in Fig. 5) would be most illustrative.

References

[1] M. Mahdavi, S. Allen and D. Baker et al., J. Nucl. Mater. 220–222 (1995) 13–24.
[2] R. Maingi, G.L. Jackson and M.R. Wade et al., Nucl. Fusion 36 (1996) 245–253.
[3] P. Mioduszewski, J. Hogan and L. Owen et al., J. Nucl. Mater. 220 (1994) 91.
[4] G. Jackson, D.R. Baker and K.L. Holtrop et al., J. Nucl. Mater. 220–222 (1995) 173–177.
[5] J. Hogan, P. Mioduszewski and L. Owen et al., J. Nucl. Mater. 196–198 (1992) 1083.
[6] C. Grisolia, P. Ghendrih, B. Pegourie and A. Grosman, J. Nucl. Mater. 196–198 (1992) 281.
[7] C. Grisolia, L. Horton and J. Ehrenberg, 15th IAEA Meeting, Seville (1994).
[8] A. Mahdavi, private communication.
[9] W. Moeller, J. Nucl. Mater. 62–164 (1989) 138.
[10] W. Moeller S. and B.M.U Scherzer, J. Appl. Phys. 64 (1988) 4860.
[11] B. Doyle, J. Nucl. Mater. 111–112 (1982) 628.
[12] V. Philipps and J. Ehrenberg, J. Vac. Sci. Technol. A, Vac. Surf Films 11 (1993) 437.
[13] K. Wilson et al., Atomic and Material Interaction Data for Fusion, Vol. 1 (1991) pp. 31–50.
[14] C. Klepper, J. Hogan and P. Mioduszewski et al., J. Nucl. Mater. 196–198 (1992) 1090–1094.
[15] D. Reiter et al., RFA-Forschungszentrum Juelich, Eirene User's Manual: Version 91 (1992).
[16] K. Audenarde, G. Emmert and M. Gordinier, J. Comput. Phys. 34 (1980) 268.